INVESTIGATION OF FLOW IN A ROTAMETER

U. Bückle, F. Durst,
B. Howe and A. Melling

Lehrstuhl für Strömungsmechanik
Universität Erlangen-Nürnberg
Erlangen, Germany

ABSTRACT

The flow in a floating element flow meter (rotameter) was studied with laser Doppler anemometry (LDA) and computational fluid dynamics (CFD). With the help of refractive index matching to eliminate optical distortion by the flow tube, the laser Doppler anemometer permitted non-intrusive velocity measurements in all regions of the flow including the immediate vicinity of the float. The computational investigation allowed an insight to the flow structure, particularly with respect to the strong velocity gradients in the gap around the float and the recirculation zone above the float. Results were obtained for various flow rates, different densities of the float material and two heights of the float in the tube.

INTRODUCTION

Flow meters find widespread application for monitoring and control of liquid and gas flows in mechanical, automotive and chemical engineering. Many types of flow meters are in common use, but floating element flow meters have proven particularly appropriate for pipe diameters smaller than 100 mm. Improvements in such meters necessitate detailed investigations of the flow, using modern techniques of experimental and computational fluid mechanics.

A floating element flow meter consists of a conical transparent vertical glass tube containing a float or "bob" (figure 1). In the present study the float is formed of cylindrical and conical sections, although spherical floats may be used in small diameter tubes. The float rises in the tube until a balance is reached between the gravitational, buoyancy and drag forces. Within the flow range of a particular flow meter (depending on the float shape and density, the tube shape and the fluid density and viscosity), the height of the float in the tube is linearly proportional to the flow rate.

In early studies of floating element flow meters, Ruppel and Umpfenbach (1930) proposed the introduction of characteristic dimensionless quantities, to permit the use of experimentally determined drag coefficients in flow meter analysis. Lutz (1959) extended these ideas by showing that the transfer of flow coefficients from one flow meter to another is possible if geometrical similarity exists.

Theories based on similarity considerations can predict the variation of the flow coefficient with the Reynolds number in the laminar and turbulent flow regimes but not in laminar-turbulent transitional flow. Detailed experimental and computational studies are needed for the transition region or in regions where fast acceleration causes relaminarization of the flow, in order to improve the accuracy of floating element flow meters. For non-intrusive velocity measurements inside the metering tube, a laser Doppler anemometer with refractive index matching was used. A computational fluid dynamics study was made with a finite volume computer program to solve the Reynolds equations, using a turbulence model to close these equations so that solutions for the entire mean flow field and for turbulence properties could be obtained.

Similarity analyses of the flow in floating element flow meters are reviewed in the next part of this paper. The two following sections describe the experimental method and the application of computational fluid dynamics to the flow. Measured and calculated velocity distributions are then presented and discussed.

ANALYSIS OF FLOATING ELEMENT FLOW METER

The forces acting on the float lead to equilibrium between the weight of the float $\rho_b g V_b$ acting downwards and the buoyancy force $\rho g V_b$ and the drag force F_d acting upwards, where V_b is the volume and ρ_b is the density of the bob, ρ is the density of the fluid and g is the gravitational acceleration:

$$\rho_b g V_b = \rho g V_b + F_d \tag{1}$$

The drag force results from the flow field surrounding the float and depends e.g. on the mean velocity profile of the upstream flow and the separation in the wake of the float. In flow analyses based on similarity principles, these influences are accounted for by empirical coefficients C_L or C_T in the drag law for

$$\text{laminar flow} \qquad F_d = C_L \mu D_b U \tag{2}$$

$$\text{turbulent flow} \qquad F_d = C_T \rho D_b^2 U^2 \tag{3}$$

where

- μ = fluid viscosity
- D_b = maximum float diameter
- U = velocity in the annular gap around the float at the minimum cross-section

The volume flow rate through the rotameter is

$$Q = \frac{\pi}{4}(D^2 - D_b^2)U \tag{4}$$

where D is the tube diameter at the top of the bob

Combining equations (1) (2) and (4) gives for laminar flow

$$Q_L = \alpha D_b^4 \frac{(\rho_b - \rho)g}{\mu} \tag{5}$$

where the constant α is defined as

$$\alpha = \frac{\pi m K}{4 C_L} \tag{6}$$

in terms of the open ratio m

$$m = \frac{D^2 - D_b^2}{D_b^2} \tag{7}$$

and a constant K characteristic of the shape of the float

Under the assumption of similarity of flows with the same Reynolds number, K can be expressed as

$$K = V_b / D_b^3 \tag{8}$$

The Reynolds number is defined as

$$Re = \frac{\rho U_{IN} D_b}{\mu} \tag{9}$$

where U_{IN} is the velocity at the rotameter inlet.

Using equation (3) instead of (2) yields for turbulent flow

$$Q_T = \beta D_b^{5/2} \sqrt{\frac{(\rho_b - \rho)g}{\rho}} \tag{10}$$

where

$$\beta = \frac{\pi m}{4} \sqrt{\frac{K}{C_T}} \tag{11}$$

At low Reynolds numbers the linear resistance law assumed in equation (2) applies and α is a constant for given m. At higher Reynolds numbers the flow is transitional or turbulent, and $\log \alpha$ decreases linearly with $\log Re$.

Curves for β against Reynolds number show a linear increase of $\log \beta$ with $\log Re$ in the laminar region, followed by a gradual transition to horizontal curves in fully turbulent flow

EXPERIMENTAL FACILITY

Test Section

The experimental test section consisted of a glass flow meter tube (Fig 1) forming part of a closed circuit flow system with by-pass, through which a glycerine solution was circulated by a pump The tube was mounted inside a rectangular plexiglass container with two planar glass windows, which was also filled with glycerine. The glycerine solution (index of refraction 1 455) minimized refractive index differences between the fluid and the tube (index of refraction 1 476), and hence reduced beam distortion due to curvature of the tube wall The viscosity of the glycerine solution was strongly temperature dependent, so that the temperature of the glycerine solution had to be held constant within ±0 3 deg C, using a cooling circuit to remove the energy input to the flow system from the pump

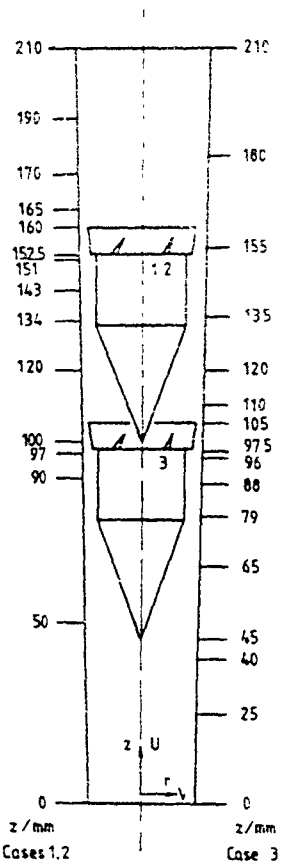

Fig 1· Flow meter geometry

Three different laminar flow cases were run (Table 1), varying the flow rate (and hence Reynolds number), the density of the float and the height of the float in the tube (measured to the top of the float).

Case	$Re = \frac{\rho U_{IN} D_b}{\mu}$	Float density g/cm^3	Float height mm
1	168	3.85	160
2	400	7.94	160
3	220	7 94	105

Table 1· Experimental Cases

Laser Doppler Anemometer

The laser Doppler anemometer (Durst et al., 1981) was a forward scatter system with a rotating diffraction grating used for beam splitting and frequency shifting, similar to the anemometer described by Oldengarm (1976). The beam from a 15 mW HeNe laser

was focused on to the diffraction grating The diffracted beams of order +1 and −1 were then focused into the measuring volume with the main lens, and the zero'th and higher order diffracted beams were masked off The half angle between the intersecting beams in the measuring volume was 5.06 deg, giving measuring volume dimensions ($1/e^2$ intensity level) of approximately 0.2 mm diameter and 2 mm length The rotational speed of the diffraction grating was adjusted to give a frequency shift exceeding twice the mean Doppler frequency

Forward scattered light from particles in the flowing glycerine was collected through a lens and focused on to an aperture in front of a photomultiplier The photomultiplier signal was preamplified, band pass filtered and fed to a frequency tracker (TSI model 1096) The analog output from the tracker is a voltage proportional to the instantaneous signal frequency, and hence to the velocity (with an offset proportional to the frequency shift) The output voltage was low pass filtered and sent to an averaging digital voltmeter (Solartron type JM 1860) from which the mean voltage was read

To minimize possible bias of the measurements resulting from drift in the speed of the rotating diffraction grating, two measurements were made at each position with positive and negative frequency shifts of the same magnitude respectively. The average of the two measurements (a voltage corresponding to zero velocity) was then subtracted from the voltage with positive frequency shift, to obtain the velocity with the correct sign. The overall uncertainty in mean velocity with this procedure was estimated to be at most 2% This accuracy in the laser Doppler measurements is adequate to describe the flow structure with sufficient detail for conclusions on improved flow meter design, and to permit comparison with computational results

COMPUTATIONAL METHOD

The numerical simulation of laminar flow in the floating element flow meter was carried out by a finite volume, multigrid computational program For the mathematical formulation of the flow problem, the conservation equations for mass and momentum in a cylindrical polar coordinate system can be written as

$$\frac{\partial}{\partial t}\rho + \frac{\partial}{\partial z}(\rho u) + \frac{1}{r}\frac{\partial}{\partial r}(\rho r v) = 0 \qquad (12)$$

$$\frac{\partial}{\partial t}(\rho u) + \frac{\partial}{\partial z}\left(\rho uu - 2\mu\frac{\partial}{\partial z}u\right) + \frac{1}{r}\frac{\partial}{\partial r}\Big(\rho ruv -$$

$$\mu r\left(\frac{\partial}{\partial r}u + \frac{\partial}{\partial z}v\right)\Big) = -\frac{\partial}{\partial z}P, \qquad (13)$$

$$\frac{\partial}{\partial t}(\rho v) + \frac{\partial}{\partial z}\left(\rho uv - \mu r\left(\frac{\partial}{\partial r}u + \frac{\partial}{\partial z}v\right)\right)$$

$$+ \frac{1}{r}\frac{\partial}{\partial r}\left(\rho rvv - 2\mu\frac{\partial}{\partial r}v\right) = -\frac{\partial}{\partial r}P, \qquad (14)$$

where ρ is the density, u, v and r, z are the velocity components and coordinate directions as defined in Fig. 1, μ is the dynamic viscosity and P is the pressure.

After discretization of these partial differential equations, following the method described by Bückle et al (1992), the resulting coupled set of equations for u, v and P is solved by a procedure based on the SIMPLE-algorithm for colocated grids (Perić et al , 1988). After a few iterations for each variable, the coefficients and source terms, which are functions of the variables, are updated (outer iterations) and the whole process is repeated until convergence, as set by a prescribed limit (typically $10^{-3} - 10^{-4}$) A "multigrid method" (Hortmann et al , 1990) was used to improve the rate of convergence of the solution. This leads to a linear increase of computing time with the number of control volumes (CV) in comparison with a quadratic increase in the case of single grid methods

The computational solution domain was one half diametral plane of the flow meter, and was subdivided into five blocks This method enabled an easy treatment of obstacles inside the solution domain, because the obstacle walls were identical with the block boundaries Each block consisted of non-uniform grids allowing a better resolution near the walls.

The coarsest grid with 920 CV was refined until a grid with 14720 CV was reached Every CV on the coarse grid was therefore divided into four CV which form the finer grid.

The boundary conditions were $u = v = 0$ along the walls and $\frac{\partial u}{\partial r} = v = 0$ along the axis of symmetry. At the input boundary the initial profile for the u-velocity was taken from the experiment, at the outlet boundary zero gradient was assumed for all dependent variables For case 2 (higher float position at higher flow rate) it was necessary to extend the solution domain by a section of parallel-walled tube of diameter equal to the outlet diameter of the flow meter tube and length 40 mm in order to obtain a converged solution

RESULTS

Measured Flow Field

Velocity profiles for the three cases of Table 1 were measured across one diameter of the tube at 15 heights. Fig. 2 shows results for case 2 Velocities are normalized by the maximum velocity at each diameter, radial distances r are normalized by the tube radius R

The entry velocity profile is flatter than that expected in fully-developed laminar pipe flow, in spite of the low Reynolds number The asymmetry must be attributed to the upstream piping At the next plane ($z = 50$ mm) the velocity profile is closer to symmetric and there is a small reduction in the maximum velocity. At $z = 90$ mm, however, a pronounced asymmetry appears again. The peak velocity is now on the other side of the tube compared with $z = 0$, suggesting the presence of some swirl in the incoming flow Just upstream of the f ($z = 97$ mm) an approximately symmetric profile is again found A depression on the tube axis indicates an upstream propagation of flow disturbance due to the float. In the plane of the float tip ($z = 100$ mm) deceleration of the flow immediately in front of the tip is very clear The velocity distribution shows a cusp on the pipe axis with a local minimum near 0.2 of the maximum velocity. The exact normalized velocity on the axis will depend on how close the measuring plane lies to the plane of the float tip, deviations of a fraction of a mm will have a strong influence on the centre-line velocity because of a steep axial velocity gradient near the stagnation point

In the next 6 planes ($z = 120, 134, 143, 151, 152.5$ and 160 mm) the progressive constriction of the flow in the decreasing gap between the float and the tube wall is clearly shown The flow area is reduced by a factor of 2.8 between the inlet station and the plane of the top of the bob, while the maximum velocity increases only by a factor of 1.9 between the same stations The difference is attributable to different velocity profiles in the tube cross-section and in the narrow gap

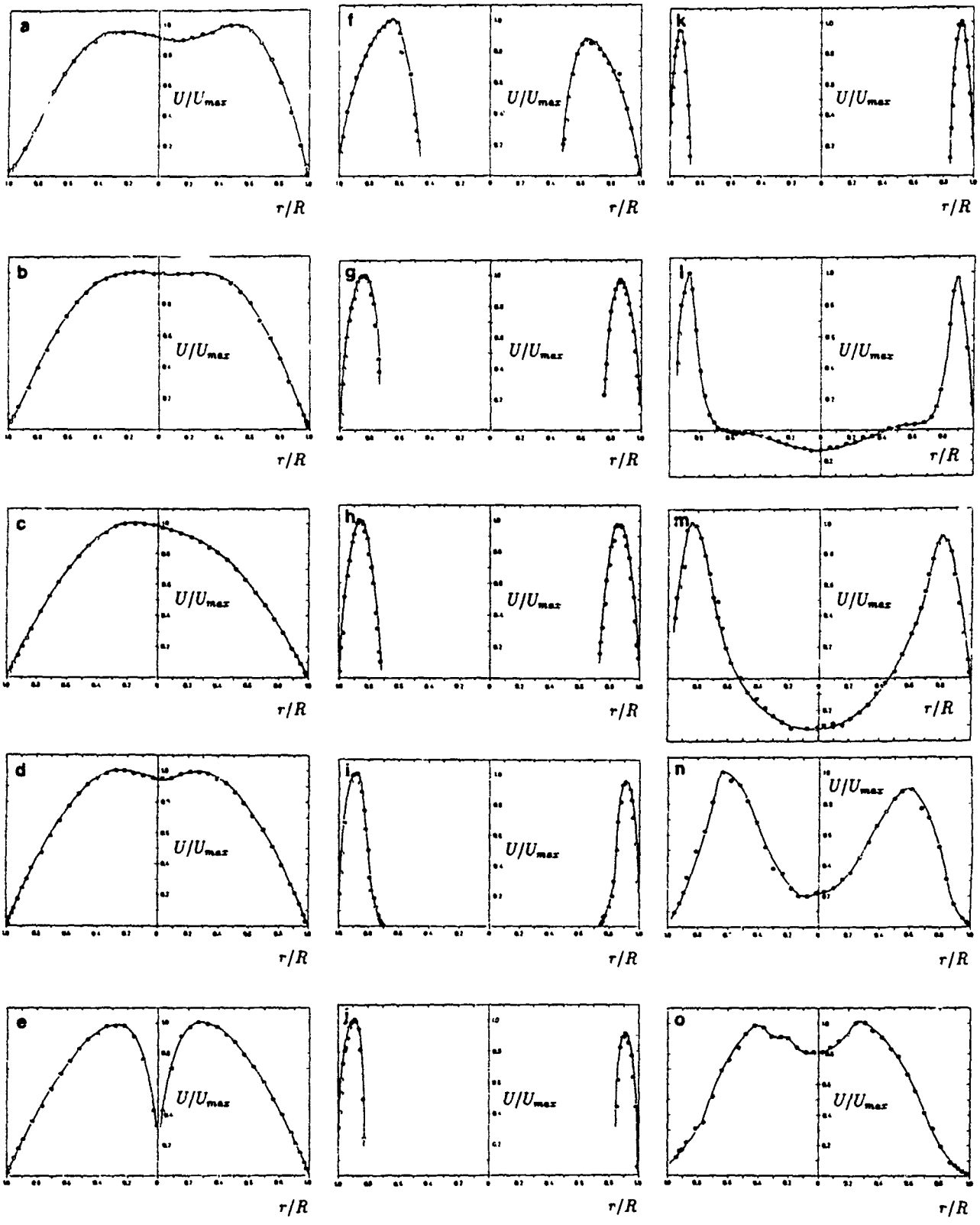

Fig. 2: Measured velocity profiles (case 2)

Fig.	z(mm)	U_{max} (cm/s)	Fig	z(mm)	U_{max} (cm/s)	Fig	z(mm)	U_{max} (cm/s)
a	0	68.2	f	120	57.1	k	160	132.2
b	50	62.3	g	134	82.5	l	165	114 8
c	90	60.1	h	143	84.3	m	175	84 3
d	97	51.5	i	151	95.1	n	190	58 3
e	100	51.8	j	152.5	117.5	o	210	52 0

A z = 165 mm the flow undergoes a rapid change as a result of the sudden increase in cross-sectional area immediatel, above the float The main flow separates from the lip of the bob, leading to a recirculation zone behind the float. Between z = 165 mm and 175 mm, the peak reverse velocity increases, indicating that the higher measuring plane passes more nearly through the centre of the recirculation zone Further downstream the cross-sectional area occupied by the main flow gradually increases and the peak forward flow velocity falls correspondingly. With increasing distance above the float, the wake region indicated by a local velocity minimum on the tube axis steadily diminishes, but at the tube outlet (z = 210 mm) there is still a significant wake region By contrast, at lower flow rate (case 1) the effect of the wake had almost disappeared.

Comparison between experimental and numerical results

The computed flow field for case 2, i e. Reynolds number 400 and the float height 160 mm is shown as a streamline plot in Fig. 3.

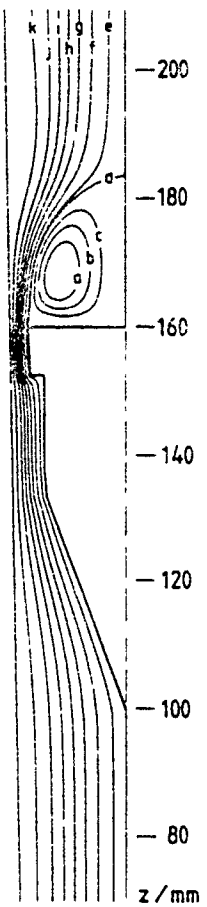

Fig 3. Computed streamlines (case 2)

Streamline	Contour value	Streamline	Contour value
a	- 0.0131	g	0.0138
b	- 0.0087	h	0.0207
c	- 0.0044	i	0.0276
d	0	j	0.0345
e	0.0015	k	0.0414
f	0.0069		

The overall features of the flow in the tube are defined, and a recirculation zone behind the "bob" and the reattachment length (i.e. the point where the zero-streamline intersects the symmetry-line) are shown. The float showed a small rotation in all flow cases which was not taken into account in the numerical study

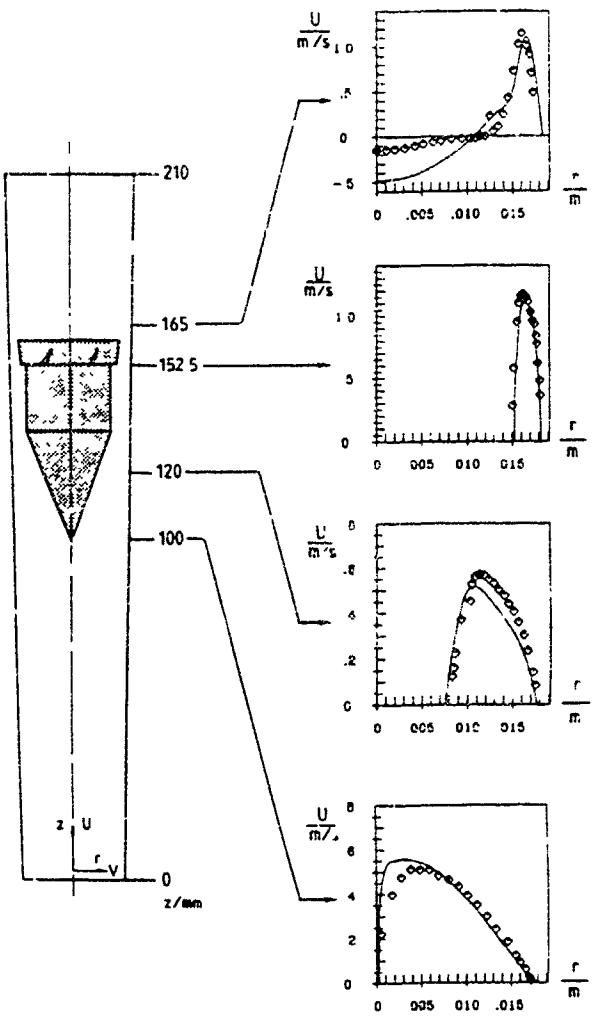

Fig. 4. Comparison of measure. and computed velocity profiles (case 2)

Experimental and computed velocity profiles over a radius of the flow meter tube are shown in Fig. 4 for case 2. The comparisons are shown in selected measuring planes in the vicinity of the float, where rapid streamwise changes in the velocity distributions occur. Profiles are shown at heights z = 100, 120, 152.5 and 165 mm, corresponding respectively to the tip, the conical portion and the lower rim of the bob, and a station just above the bob.

At the first comparison station (z = 100) the computations indicate exactly zero velocity on the axis, corresponding to a stagnation point at the float tip. The measurements show a low but non-zero axial velocity at the tip. The deviation from zero is probably attributable to two factors: slight unsteadiness in the position of the float, even under nominally steady flow conditions, and smearing of the radial distribution of velocity along the length of the measuring volume, which was unavoidably rather long in comparison with the radius. This effect is also apparent at radii up to about 5 mm, where the computations show a notably steeper velocity gradient than the measurements. The measured and computed

peak velocities in the profiles agree rather well, although the peak of the measured profile is located at a larger radius At larger radii, where the velocity decreases more gradually toward the wall, computed and measured profiles are in close agreement

In the strongly converging annulus between the bob and the tube wall, 20 mm above the float tip (z = 120 mm), the computations reproduce the trend of the measured results well, although there are some noteworthy deviations The measured points in the region of rising velocity adjacent to the bob are displaced to higher radius relative to the computed velocity profiles In the region of falling velocity near the flow meter wall, however, computed and measured results deviate more noticeably The discrepancy is linked with an apparent deviation from mass conservation in the measurements, which is partly attributable to flow asymmetry The profiles in Fig 2 indicate asymmetry in axial velocity at equal radii on either side of the axis up to 10%. Possible asymmetry along diameters inclined to the main measurement planes could also have contributed to the mass imbalance

At z = 152 5 mm. measured and computed velocities appear to be in close agreement, except for some deviation in the peak velocities The confinement of the flow in the narrow annular gap in this plane, however, makes any differences difficult to resolve.

5 mm above the float (z = 165 mm) the flow is characterized by a strong upward flow in an annular region near the flow meter tube wall and a recirculation region around the axis occupying almost half the tube cross-section The forward velocities show a reasonably good match between computations and measurements, but there is a very marked discrepancy in the recirculation zone, where the measured maximum reverse velocity is only one-third of the computed value and the measured recirculation region extends radially to only 9 mm compared with 11 mm computationally Between 9 mm and 14 mm in the measurements, however, is an area of almost zero mean velocity, so that the region of forward velocity is actually smaller than in the computations.

As a whole, good agreement is obtained between experimental and numerical results, apart from the separation region after the float Effects caused by rotation of the floating element and asymmetry of the oncoming velocity profile could not be taken into account in the axi-symmetric flow predictions A possible further cause of discrepancies is an insufficient number of numerical nodes downstream of the float, where the shear layer develops from the upper edge of the floating element

CONCLUSIONS

This paper emerges from a sequence of studies at the authors' institute related to improvements of volume and mass flow meters by modern experimental, analytical and numerical techniques of fluid mechanics. The complementary use of these techniques provides the best insight into the details of the flow and their influence on the accuracy of volume or mass flow metering.

The results show that the computational fluid dynamics (CFD) code is capable of reproducing the features of the flow indicated by the measurements by laser Doppler anemometry Quantitative disagreement between results by the two methods does not invalidate this conclusion, but points up the difficulties of the experimental and computational tasks, particularly in the narrow annular gap existing in some geometrical planes The results give a convincing demonstration of the utility of modern tools of computational and experimental fluid mechanics to improving the analysis and design of flow meters which traditionally has had to be treated semi-empirically. A useful extension of the work would be a study for Reynolds numbers appropriate to turbulent flow in the flow meter

ACKNOWLEDGEMENTS

Partial financial support was obtained for this study by the Rota-Company This support is thankfully acknowledged

REFERENCES

Bückle, U., Durst, F., Howe, B. and Melling, A. (1992) Investigation of a floating element flow meter Submitted for publication in Flow Measurements and Instrumentation.

Durst, F., Melling, A. and Whitelaw, J.H. (1981) Principles and Practice of Laser-Doppler Anemometry Academic Press, London (2nd ed)

Hortmann, M., Perić, M and Scheuerer, G.(1990) Finite volume multigrid prediction of laminar natural convection benchmark solutions, International Journal for Numerical Methods in Fluids 11, 189-207.

Lutz, K. (1959) Die Berechnung des Schwebekörper-Durchflußmessers, Regelungstechnik, 10, 355-360.

Oldengarm, J. (1976) Development of rotating diffraction gratings and their use in laser anemometry, Optics & Laser Tech 69

Perić, M., Kessler, R. and Scheuerer, G. (1988) Comparison of finite volume numerical methods with staggered and colocated grids, Computers and Fluids 16, 389-403

Ruppel, G. and Umpfenbach, K.J. (1930) Strömungstechnische Untersuchungen an Schwimmermesse.n, Technische Mechanik und Thermodynamik, 1, 225-233, 257-267, 290-296